DIFFUSION-REACTION OF CO, NO AND O_2 IN AUTOMOTIVE EXHAUST CATALYSTS

Simulations of simultaneous diffusion and reaction of CO, NO and O_2 in the pores of three-way catalysts are matched with experimental data to give estimates of intrinsic kinetics of CO-O_2 and CO-NO reactions. A steady state one-dimensional model for the monolith converter is developed, including heat and mass transfer between the bulk gas and the solid, and diffusion-reaction within the pores. Non-isothermality of the pores is accounted for by the internal-isothermal model, so that at any axial position within the converter they are isothermal, but at a temperature different from that of the bulk gas. Predictions of the model compare well with experiments.

J. W. Kress
N. C. Otto
M. Bettman

Ford Motor Company
Dearborn, Michigan 48121

J. B. Wang
and
A. Varma

University of Notre Dame
Notre Dame, Indiana 46556

Current converters catalytically control only CO and hydrocarbons from automotive exhausts. The NO standards are presently met by exhaust gas recirculation (EGR) and by manipulating engine operating conditions. In the near future, NO and fuel economy standards will become sufficiently stringent that current methods for NO control will have to be replaced by catalytic ones (1).

It is envisioned that catalysts which simultaneously control CO, hydrocarbons and NO will operate close to stoichiometry -- although complicating oxidizing and reducing transients will be present in the feed (2-7). We here report some preliminary steps that have been taken in the direction of modeling steady state monolithic converters using three-way catalysts.

The reaction kinetics in as complex an environment as automotive exhaust, with a multicomponent catalyst, are simply not known at this time. With a thermally aged commercial three-way monolith catalyst (aged at 790°C for 16 hours in burner exhaust at ~ stoichiometric conditions), an experimental steady state data base has been acquired for various subsystems such as CO-NO-O_2, in the presence of 20 ppm SO_2, 12% CO_2, 10% H_2O and N_2 as the diluent (8). In each of the subsystems, the number of possible chemical reactions is considerably reduced. Certain likely kinetic expressions with adjustable parameters are used in this work, and values of these parameters are selected by an optimization procedure described later.

Specifically, in the CO-NO-O_2 subsystem, the following three reactions appear to be the most important:

$$CO + \frac{1}{2} O_2 \rightarrow CO_2 \qquad (1)$$

$$CO + NO \rightarrow \frac{1}{2} N_2 + CO_2 \qquad (2)$$

$$5CO + 2NO + 3H_2O \rightarrow 2NH_3 + 5CO_2 \qquad (3)$$

Further, since NH_3 is formed to a relatively small extent in the data sets analyzed, for a preliminary investigation, only the first two are considered in this work. The experimental data are utilized to invoke optimization of intrinsic rate parameters by a Simplex procedure coupled with diffusion-reaction within the pores. With the optimized parameters having thus been obtained, the converter model predictions are tested. The comparison of the model with experiments is rather good, especially for CO.

THE BASIC EQUATIONS

The intrinsic reaction rate expressions for reactions (1) and (2), containing intrinsic rate parameters, are assumed. The simultaneous diffusion and reaction of CO, NO, and O_2 occurring in the pores of washcoat

0065-8812-80-3675-0201-$01.15.

are governed by the balance equations:

$$D_1 \frac{d^2C_1}{dy^2} = \frac{k_1C_1C_3}{(1+K_1C_1+K_2C_2)^2} + \frac{k_2C_1C_2}{(1+K_1C_1+K_2C_2)^2} \quad (4)$$

$$D_2 \frac{d^2C_2}{dy^2} = \frac{k_2C_1C_2}{(1+K_1C_1+K_2C_2)^2} \quad (5)$$

$$D_3 \frac{d^2C_3}{dy^2} = \frac{\frac{1}{2}k_1C_1C_3}{(1+K_1C_1+K_2C_2)^2} \quad (6)$$

where k_1, k_2 are the intrinsic reaction rate constants of reactions (1) and (2), respectively, and y is the distance within the pore from the pore-mouth. Subscripts 1, 2, and 3 represent CO, NO, and O_2, respectively. The associated general boundary conditions are:

$$\frac{dC_i}{dy} = 0 \quad ; \quad y=0 \quad (7)$$

$$D_i \frac{dC_i}{dy} = k_{gi}(C_{ig}-C_{is}) \quad ; \quad y=L \quad (8)$$

for $i = 1 \rightarrow 3$.

Introducing the dimensionless quantities,

$$u_i = x_i/x_{ig} \ , \ s=y/L \ , \ Bim_i=k_{gi}L/D_i \ , \quad K_{ig}=K_i\rho_s x_{ig} \ , \ \phi^2_{ijk}=k_iL^2\rho_s x_{jg}/D_k \quad (9)$$

where

$$\rho_s=1/R_gT_s \ , \ \rho_g=1/R_gT_g \ , \ x_i=C_i/\rho_s \ , \quad \text{and} \ x_{ig}=C_{ig}/\rho_g \quad (10)$$

eqns. (4) to (8) reduce to dimensionless form

$$\frac{d^2u_1}{ds^2} = \frac{\phi^2_{131}u_1u_3+\phi^2_{221}u_1u_2}{(1+K_{1g}u_1+K_{2g}u_2)^2} \quad (11)$$

$$\frac{d^2u_2}{ds^2} = \frac{\phi^2_{212}u_1u_2}{(1+K_{1g}u_1+K_{2g}u_2)^2} \quad (12)$$

$$\frac{d^2u_3}{ds^2} = \frac{\frac{1}{2}\phi^2_{113}u_1u_3}{(1+K_{1g}u_1+K_{2g}u_2)^2} \quad (13)$$

with boundary conditions

$$\frac{du_i}{ds} = 0 \quad ; \quad s=0$$
$$\frac{du_i}{ds} = Bim_i\left(\frac{\rho_g}{\rho_s} - u_{is}\right) \quad ; \quad s=1 \quad (14)$$

The integral monolith converter is modeled as an adiabatic plug-flow reactor, with heat and mass transfer between the gas and the washcoat surface, and diffusion-reaction within the pores. The complete mass and heat balance equations are

Mass Balance:

$$-\rho_g \frac{dx_{ig}}{dz} = \frac{k_{gi}A}{v}(\rho_g x_{ig}-\rho_s x_{is}), \ i=1,2,3 \quad (15)$$

$$-\rho_g \frac{dx_{ig}}{dz} = \frac{A}{v}R_i \quad (16)$$

where R_i is the rate of reaction of the i-th species, and z is the distance from the converter inlet.

Energy Balance:

$$\rho_g C_p \frac{dT_g}{dz} = \frac{A}{v}\sum_{j=1}^{n_r}(-\Delta H_j)r_j \quad (17)$$

$$-\rho_g C_p \frac{dT_g}{dz} = \frac{hA}{v}(T_g-T_s) \quad (18)$$

where r_j is rate of the j-th reaction and n_r is number of reactions considered, which is 2 in present case. The meanings of various terms are defined in the Notation.

The initial conditions for eqns (15) to (18) are:

$$x_{ig} = x^0_{ig} \quad ; \quad z=0$$
$$T_g = T^0_g \quad ; \quad z=0 \quad (19)$$

Eqns. (11) to (19) accommodate changes in gas and surface densities caused by axial temperature variations. The mass and heat transfer coefficients are calculated from engineering correlations (9,10) as a function of gas temperature, and of axial position in the converter; they allow for turbulent flow near the inlet, gradually developing into laminar flow. Other correlations of these transfer coefficients are also reported in literature (11-13).

OPTIMIZATION OF INTRINSIC RATE PARAMETERS

It should be noted that with an integral reactor, intrinsic kinetic data cannot be obtained experimentally. Therefore, the modeling of the reaction system is resorted to get the optimized intrinsic rate parameters based on the experimental data base. The assumed intrinsic reaction rate expressions for reactions (1) and (2) contain intrinsic rate parameters. The temperature independent parts of these rate parameters and Biot number of CO for external mass transport and the corresponding activation energies which are to be optimized are listed in Table 1.

TABLE 1.

Intrinsic Reaction Rate Parameters to be Optimized

X_1:	product of the pre-exponential part of k_1 and L^2
X_2:	product of the pre-exponential part of k_2 and L^2
X_3:	pre-exponential part of K_1
X_4:	ratio of pre-exponential part of K_1 to that of K_2
X_5:	activation energy of k_1
X_6:	activation energy of k_2
X_7:	activation energy of K_1
X_8:	difference of activation energies of K_1 and K_2; i.e., E (K_2)-E (K_1)
X_9:	temperature independent part of Bim_1

The experimental data base of the subsystem of CO-NO-O_2 was first fitted (8) with a computer model of the catalytic converter, including heat and mass transfer from the bulk gas to the washcoat surface, by a Simplex optimization procedure (14,15). This produced what in sequel will be termed "experimental surface reaction rates". Then, the system of three coupled nonlinear ordinary differential eqns. (11) to (13) for the pore is numerically solved by orthogonal collocation technique (16,17). The calculated surface reaction rates are then compared with the experimental ones obtained as described above.

The sum of the squares of differences between calculated and experimental rates for the three species, divided by the observed values is termed as the "object function" and is an indication of the goodness of fit. A limited set of data points (all with less than 2% conversion of NO to NH_3), chosen for probable reliability and appropriate ranges of input variables, was selected. A sampled data point consists of inlet temperature, redox potential, compositions of CO, NO, and O_2. The redox potential, a measure of the exhaust stoichiometry, of the reacting gas mixture is obtained by dividing the sum of the equivalent reducing components of the mixture by the sum of the oxidizing components. Thus,

$$\text{Redox Pot., } R = \frac{[CO]}{[NO] + 2[O_2]} \qquad (20)$$

Therefore, R > 1 represents an overall reducing gas mixture and R = 1, a stoichiometric gas mixture.

A total of twelve composition data points shown in Table 2,

TABLE 2.

Inlet Conditions for Data Points Used for Parameter Optimization
with 10% H_2O, 12% CO_2, 20 ppm SO_2, balance N_2
Space Velocity: 50,000hr^{-1}

inlet temp,°F	%CO	%O_2	ppm NO	inlet redox pot.
1107	0.300	0.110	1490	0.813
904	0.300	0.097	1509	0.870
902	1.490	0.750	1499	0.903
1107	0.300	0.110	988	0.941
1100	0.290	0.099	988	0.977
1096	1.520	0.750	500	0.981
904	0.300	0.097	997	1.021
903	1.020	0.390	2003	1.040
902	0.535	0.217	492	1.107
903	1.020	0.355	1998	1.121
1096	1.480	0.500	2500	1.184
1100	0.310	0.099	505	1.247

each with five different relevant surface temperatures--900°, 950°, 1000°, 1050° and 1100°F, was chosen as the data base. This set of twelve data points covers wide ranges of bulk gas temperature, compositions, and redox potential representative of the conditions in the converter. A Simplex optimization was performed to minimize the object function over the data base, relative to all conceivable variations of all the intrinsic rate

parameters within a chosen large but limited domain for each parameter. The initial estimates of these intrinsic rate parameters were set equal to the corresponding values of conventional oxidation catalyst (COC) model (9,10). Activation energies were initially set to some average, reasonable values, unless there existed some specific prior information. The Simplex minimization process changes one, or several, of the parameters, repeats the computation of the object function for the five relevant surface temperatures and the twelve data points; and continues doing this until a minimum value of the object function in the parameter space is found--within a relative change of 10^{-5} for all the parameters.

The calculated and experimental surface reaction rates for each species using the optimized rate parameters are shown in Figure 1.

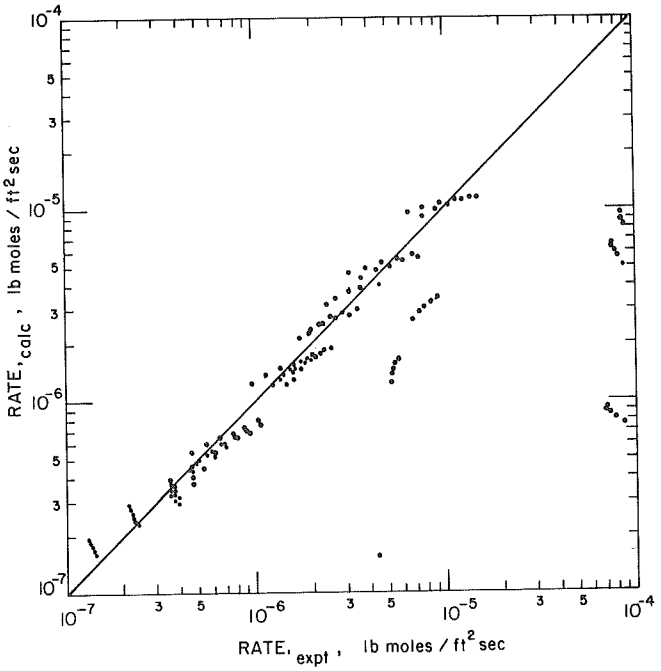

A total of 180 pairs of rates are compared. As can be seen the comparison is reasonably good--most of the points fall in the neighborhood of the 45°diagonal with the exception of a few points which are on the reducing side of the stoichiometry of exhaust gas mixtures.

CONVERTER MODEL PREDICTIONS

With the optimized intrinsic reaction rate parameters having thus been obtained, the integral monolith converter was modeled as a plug-flow reactor, eqns. (15) to (18), with heat and mass transfer between the gas and the washcoat surface, and diffusion-reaction within the pores.

At axial location z, for each gas phase composition and temperature, there are corresponding surface compositions and temperature, which are obtained as described below.

Eqns. (15) and (16) are coupled to give

$$k_{gi}(\rho_g x_{ig} - \rho_s x_{is}) - R_i = 0 \qquad (21)$$

Also, eqns. (17) and (18) lead to

$$\sum_{j=1}^{n_r} (-\Delta H_j) r_j + h(T_g - T_s) = 0 \qquad (22)$$

For each gas phase temperature and compositions, an initial estimate of the corresponding surface temperature is guessed, and thus the surface compositions are computed from the diffusion-reaction within the pores, eqns. (11) to (14). The resulting surface temperature and compositions are substituted into eqns. (21) and (22) to see whether eqn. (22) is met or not. If not, a new guess of the surface temperature is made from (22), and the same procedure is repeated until eqn. (22) is satisfied. Then, the present surface temperature and compositions are the exact ones corresponding to the gas phase temperature and compositions at a particular location z.

With the surface temperature and compositions having been obtained, the differential equations in x_{ig} and T_g of (15) and (18) are then numerically integrated to yield the gas phase temperature and compositions at the outlet of converter. Experimental data sets for the integral converter, other than those used to obtain the intrinsic rate parameters, are now utilized to test the converter model predictions. A comparison of the model with experiments is shown in Table 3.

TABLE 3.

Comparison of Calculated and Experimental Values

A. Converter Inlet

Set	Temp,°F	%CO	$\%O_2$	ppm NO	redox pot.
1	1096	1.345	0.682	1803	0.871
2	902	0.482	0.194	1367	0.916
3	909	0.909	0.365	2283	0.948
4	902	0.486	0.196	906	1.006
5	904	0.273	0.088	906	1.021
6	1107	0.473	0.090	1821	1.306

B. Converter Outlet

Set	Conversions, %				
	CO		NO		
	Expt.	Calc.	Expt.	Calc.	Temp,°F
1	100	100	14.3	22.3	1311
2	100	99.8	76.3	69.9	985
3	100	99.9	76.5	78.2	1065
4	99.1	97.8	98.0	91.4	983
5	98.4	95.1	100	91.5	950
6	74.4	76.6	92.2	99.9	1174

It appears that the predictions of the model are rather good, especially for CO.

To get a clearer picture along the converter length, bulk temperature and composition profiles are examined in Figures 2 and 3.

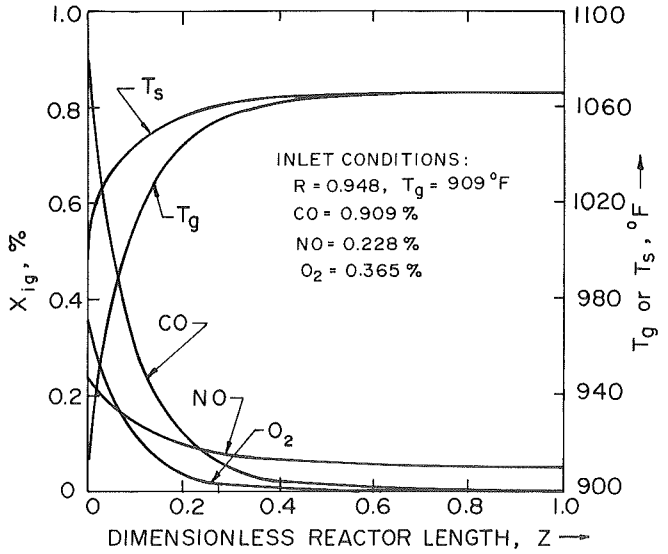

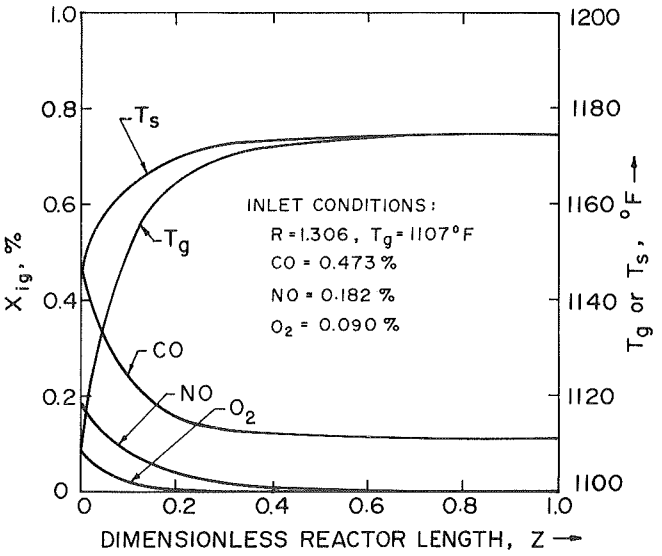

For the oxidizing gas mixture CO is completely used up, while in overall reducing atmosphere O_2 is used up completely. As can be seen there is appreciable temperature gradient between the bulk and surface near the inlet, and both the temperature and composition profiles quickly develop to their final outlet values after the first 50% of monolith length.

SOME FURTHER OBSERVATIONS ON THE DIFFUSION-REACTION BEHAVIOR IN THE PORES

To obtain some qualitative insight of the conditions to which diffusion-reaction inside the pores corresponds, since the system is non-isothermal, standard non-isothermal, effectiveness factor-Thiele modulus plots for reactions (1) and (2) were made for a variety of realistic bulk gas phase compositions. This was done by adding one more equation and B.C. to the mass and heat balance equations in the pores:

$$\lambda\frac{d^2T}{dy^2} = \frac{-(-\Delta H_1)k_1C_1C_3-(-\Delta H_2)k_2C_1C_2}{(1+K_1C_1+K_2C_2)^2} \qquad (23)$$

with BCs

$$\frac{dT}{dy} = 0 \quad , y=0 \quad , \quad \lambda\frac{dT}{dy} = h(T_g-T_s) \quad , y=L \quad (24)$$

Eqns. (4) to (8) and (23), (24) were then simultaneously solved numerically by orthogonal collocation technique. The effectiveness factor η is defined as the ratio of the actual rate of reaction to that which would prevail under conditions of no transport limitations. Figures 4 to 8

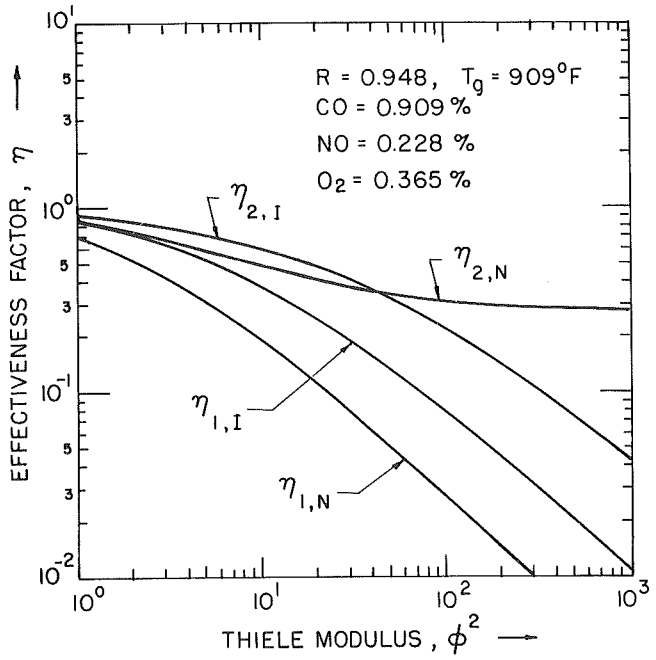
R = 0.948, T_g = 909°F
CO = 0.909 %
NO = 0.228 %
O_2 = 0.365 %
$\eta_{2,I}$
$\eta_{2,N}$
$\eta_{1,I}$
$\eta_{1,N}$
EFFECTIVENESS FACTOR, η
THIELE MODULUS, ϕ^2

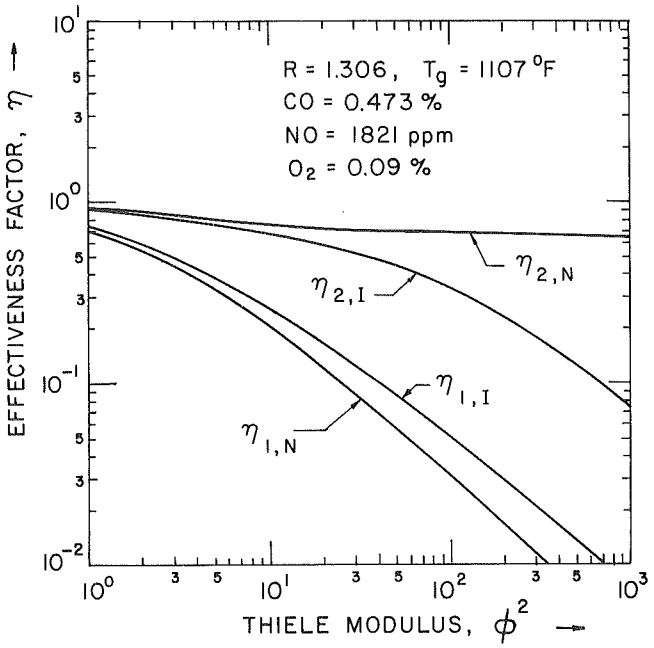
R = 1.306, T_g = 1107°F
CO = 0.473 %
NO = 1821 ppm
O_2 = 0.09 %
$\eta_{2,N}$
$\eta_{2,I}$
$\eta_{1,I}$
$\eta_{1,N}$
EFFECTIVENESS FACTOR, η
THIELE MODULUS, ϕ^2

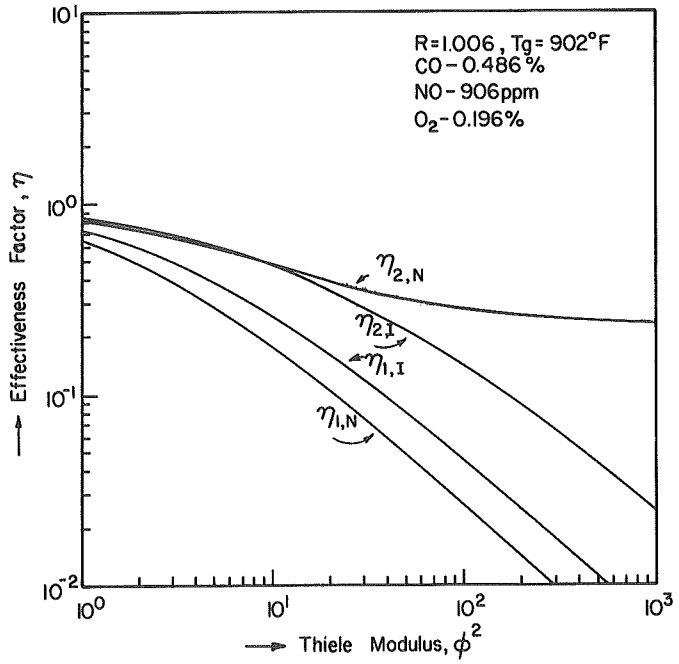
R=1.006, Tg= 902°F
CO-0.486%
NO-906ppm
O_2-0.196%
$\eta_{2,N}$
$\eta_{2,I}$
$\eta_{1,I}$
$\eta_{1,N}$
Effectiveness Factor, η
Thiele Modulus, ϕ^2

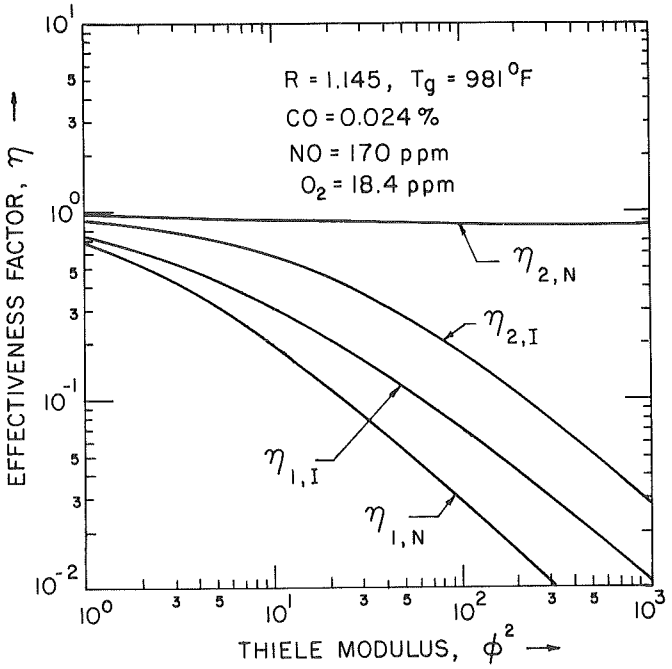
R = 1.145, T_g = 981°F
CO = 0.024 %
NO = 170 ppm
O_2 = 18.4 ppm
$\eta_{2,N}$
$\eta_{2,I}$
$\eta_{1,I}$
$\eta_{1,N}$
EFFECTIVENESS FACTOR, η
THIELE MODULUS, ϕ^2

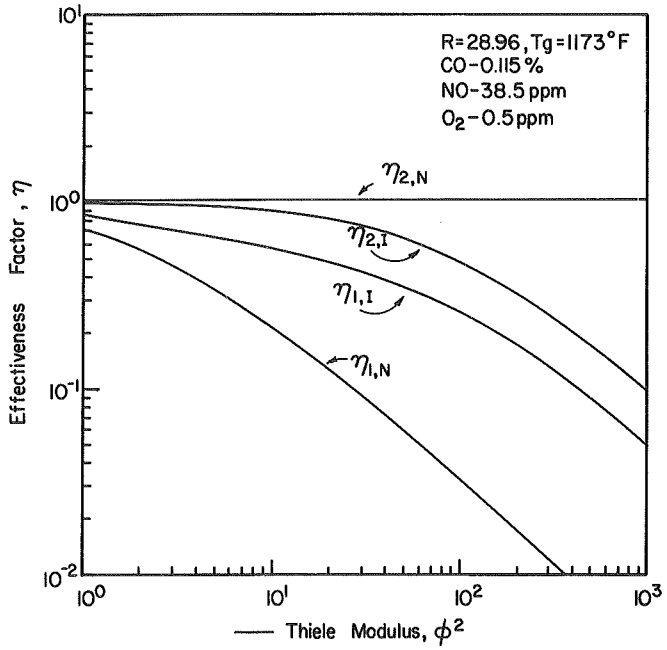

show several such curves; the expected Thiele modulus values corresponding to the bulk conditions and diffusion-reaction inside the pores are also shown in the captions. It is seen that NO reaction within the pores is intermediate between kinetic and pore-diffusion control, while the CO reaction is intermediate between pore-diffusion control and external mass-transfer control. Some works investigating uniqueness and multiplicity behavior of steady states of a reaction following the bimolecular Langmuir-Hinshelwood mechanism were reported in literature (18,19). Here, for diffusion-reaction of CO, NO, and O_2 in automotive exhaust three-way catalysts, at conditions covering a wide range of bulk temperature, compositions, and redox potential at the inlet or the middle of the converter, as exhibited in Figures 4 to 8, multiple steady states were not found.

As can be noted, in the optimization of parameters and the converter model predictions isothermal diffusion-reaction within the pores was assumed. But the whole system of catalytic converter is non-isothermal, for which the pore-diffusion problem is solved by the internal isothermal model. It is worth investigating whether the internal isothermal model within the pores is valid here or not. Thus, temperature and concentration profiles within the pore are plotted in Figure 9.

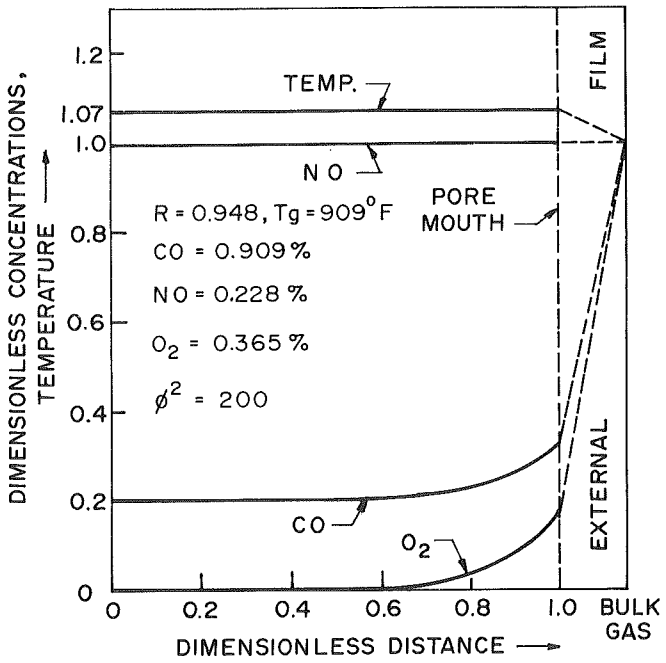

As seen in the figure, the temperature profile is virtually constant within the entire pore. The internal isothermal model was rigorously justified for most gas-solid catalytic reactions recently (20), and the present work again shows that such a model is a good one. It is recalled that the parameters were optimized using a constant pore temperature, and the converter model utilizes the internal isothermal model for pore-diffusion --both these procedures are thus fully justified. It is worth remarking that using the internal isothermal model for pore diffusion, rather than the complete differential balance for energy, eqns. (23) and (24), results in a substantial saving of computation time.

The fact that the NO concentration is very close to unity as shown in Figure 9, and the selectivity favors the CO-O_2 reaction over the CO-NO reaction explains that the non-isothermal effectiveness factor of NO is relatively close to unity, as shown in Figures 4 to 8. Further calculations show that the asymptotic slope of the NO η vs ϕ^2 curves eventually approaches -1 for very large ϕ^2, which is well-known and in agreement with the theory of diffusion and reaction (20,21).

Also, as seen in Figures 4 to 8, the non-isothermal effectiveness curves differ substantially from those of the fully isothermal ones. This points to the necessity of including heat transfer between the external monolith surface and the bulk gas--which is precisely what is done in the internal isothermal model.

CONCLUDING REMARKS

In summary, intrinsic rate parameters for the CO-O_2 and the CO-NO reactions were determined by fitting the results of a diffusion-reaction model with experimental rate data obtained before (8). These parameters were then used to predict the performance of the monolith converter, which was compared with experimental results. The converter model was a one-dimensional model, coupled with heat and mass transfer between the gas and the solid, and diffusion-reaction within the pores of the washcoat. The importance of pore diffusion was shown, and it was also shown that the internal isothermal model is quite adequate for the pore diffusion-reaction problem.

CO-O_2 reaction is favored over the CO-NO reaction in the temperature range of interest. For the overall oxidizing gas mixture both the selectivity and calculated surface reaction rates based on the optimized rate parameters gave better fit with experimental results.

Multiple steady states were not observed for the representative conditions at the inlet or the middle of the converter. The non-isothermal effectiveness of NO is relatively close to unity which is due to the fact that the NO concentration inside the pore is very close to unity and CO-O_2 reaction is favored selectively.

It is a difficult task to extract true kinetic parameters from integral reactor experimental data. This is so because a reactor model is required. Intrinsic kinetics are better obtained in gradientless reactors (22), such as a continuous-stirred-tank catalytic reactor (23) or a fixed-bed recycle reactor (24-26). Indeed, we are presently using a recycle reactor to experimentally obtain intrinsic kinetics. However, in the absence of intrinsic kinetics obtained from such reactors, the present study provides some estimates of the kinetic parameters and is the best that can result from the experimental data of an integral reactor. The comparisons of predicted and experimental reactor conversions (Table 3) are good, and so provide the hope that overall kinetics are perhaps not too different from those established here.

ACKNOWLEDGEMENT. This work was supported by the Department of Energy, as part of a joint research program between Ford Motor Company and the University of Notre Dame.

NOTATION

A	geometric surface area
Bi_m	Biot number for external mass transport
C	reactant concentration
C_p	heat capacity of exhaust gas mixture
D	effective diffusivity
E	activation energy
ΔH	heat of reaction
h	heat transfer coefficient of gas mixture
K_i	adsorption rate constant of the i-th species
k_g	mass transfer coefficient
k_j	the j-th reaction rate constant
L	pore length
n_r	number of reactions involved
R	redox potential defined by eqn. (20)
R_g	gas constant
R_i	rate of reaction of the i-th species
r_j	rate of the j-th reaction
s	dimensionless distance, y/L
T	temperature
u	dimensionless concentration, x/x_g

v actual space velocity

X_i intrinsic rate parameter to be optimized

x_i mole fraction of reactant i in the pore, C_i/ρ_s

x_{ig} mole fraction of reactant i in the gas phase, C_{ig}/ρ_g

y pore distance

z dimensionless reactor distance

Greek Symbols

ρ molar density of gas mixture

ϕ_{ijk} Thiele modulus, $[k_i L^2 \rho_s x_{jg}/D_k]^{1/2}$

η effectiveness factor

λ effective thermal conductivity

Subscripts

g gas phase

m related to mass transfer

s solid surface

Superscripts

$^\circ$ inlet condition

LITERATURE CITED

1. Kummer, J. T., Prog. Energy Combust. Sci., 6 (in press).
2. Gandhi, H. S., A. G. Piken, M. Shelef and R. G. Delosh, "Laboratory Evaluation of Three-Way Catalysts," SAE Transactions, Sec. 2, 85, 901 (1976).
3. Gandhi, H. S., A. G. Piken, H. K. Stepien, M. Shelef, R. G. Delosh and M. E. Heyde, "Laboratory Evaluation of Three-Way Catalysts, Part II," Paper no. 770196, presented at the Society of Automotive Engineers meeting, Detroit, February (1977).
4. Hegedus, L. L., J. C. Summers, J. C. Schlatter and K. Baron, Jl. Catalysis, 56, 321 (1979).
5. Schlatter, J. C., R. M. Sinkevitch and P. J. Mitchell, "A Laboratory Reactor System for Three-Way Catalyst Evaluation," General Motors Research Publication GMR-2911 (1979).
6. Yao, Y.-F. Y., "The Effect of CO_2 in Automotive Exhaust Catalysts," presented at the Sixth North American Meeting of the Catalysis Society, Chicago, March (1979).
7. Schlatter, J. C. and P. J. Mitchell, "Three-Way Catalyst Response to Transients," General Motors Research Publication GMR-3053 (1979).
8. Bettman, M. and M. D. Johnson, "Progress Report on Three-Way Catalyst Modeling-I" Ford Motor Company Technical Report No. SR-78-28 (1978).
9. Otto, N. C., "A Mathematical Model for Monolithic Catalytic Converters," Ford Motor Co. Technical Report No. SR-74-85 (1974).
10. Otto, N. C., "Application of a Mathematical Model for Noble Metal Catalytic Converters," Ford Motor Co. Technical Report No. SR-74-86 (1974).
11. Votruba, J., J. Sinkule, V. Hlaváček and J. Skrivánek, Chem. Eng. Sci., 30, 117 (1975).
12. Hegedus, L. L., "Effects of Channel Geometry on the Performance of Catalytic Monoliths," General Motors Research Publication GMR-1370 (1973).
13. Hawthorne, R. D., "Afterburner Catalysts --Effects of Heat and Mass Transfer Between Gas and Catalyst Surface," Shell Development Co., Emeryville, CA. (1972).
14. Nelder, J. A. and R. Mead, The Computer Jl., 7, 308 (1965).
15. Spendley, W., G. R. Hext and F. R. Himsworth, Technometrics, 4, 441 (1962).
16. Finlayson, B. A., The Method of Weighted Residuals and Variation Principles, Academic Press, New York (1972).

17. Villadsen, J. and M. Michelsen, Solutions of Differential Equation Models by Polynomial Approximations, Prentice-Hall, Englewood Cliffs, New Jersey (1978).

18. Pereira, C. J. and A. Varma, Chem. Eng. Sci., 33, 1645 (1978).

19. Hegedus, L. L., S. H. Oh and K. Baron, AIChE Jl., 23, 632 (1977).

20. Pereira, C. J., J. B. Wang and A. Varma, AIChE Jl., 25, 1036 (1979).

21. Aris, R., The Mathematical Theory of Diffusion and Reaction in Permeable Catalysts. Volumes I and II, Claredon Press, Oxford (1975).

22. Weekman, V. W., Jr., AIChE Jl., 20, 833 (1974).

23. Tajbl, D. G., J. B. Simmons and J. J. Carberry, Ind. Eng. Chem. Fundls., 5, 171 (1966).

24. Bennett, C. O., M. B. Cutlip and C. C. Yang, Chem. Eng. Sci., 27, 2255 (1972).

25. Berty, J. M., Chem. Eng. Prog., 70 (5), 78 (1974).

26. Paspek, S. C., A. Varma and J. J. Carberry, Chem. Eng. Edn. (in press).

Emission Control from Stationary Power Sources: Technical, Economic and Environmental Assessments

Alfred J. Engel, Stevan M. Slater and James W. Gentry, *editors*

H. J. Annegarn
V. P. Aneja
H. M. Barnes
S. E. Bauman
M. Bettman
J. S. Bowen
K. Y. Chen
Z. Chiba
W. W. Choi
L. T. Cupitt
Robert H. Dahlin
Barton Dahneke
Cliff I. Davidson
E. R. Denoyer
J. L. Durham
Robert W. Elias
G. C. England
M. Ernst
Karsten Felsvang
W. H. Fischer
G. L. Fisher
Robert A. Fjeld
G. Flament
Kochy Fung
H. S. Gandhi
Randall O. Gauntt
Glen E. Gordon
Daniel Grosjean
G. T. Hall
R. E. Hall
T. L. Hayes
M. P. Heap
Steven Heisler
George Hidy
E. B. Higginbotham
R. C. Hoke
Keith House
M. M. Johnston
Gary D. Jones
Steven M. Kaplan
T. R. Keyser
S. E. Kirton
Gregory S. Kowalcyzk
J. W. Kress
D. P. Kromka
R. C. Ku
C. E. Lai
A. C. D. Leslie
K. J. Lim
Paul J. Lioy
Andrew R. McFarland
K. L. Maloney
H. B. Mason
J. F. Meagher
Charles A. Mims
J. David Mobley
Peter Mueller
D. F. S. Natusch
Matthew Neville
N. C. Otto
J. H. Overton, Jr.
Leonard K. Peters
D. W. Pershing
Wade H. Ponder
B. A. Prentice
Richard J. Quann
Kenneth A. Rahn
L. A. Ruth
Adel A. Sarofim
D. Schuykens
Ja-an Su
D. R. Taylor
T. J. Truex
Philip Varghese
A. Varma
J. B. Wang
L. R. Waterland
W. B. Williamson
W. E. Wilson, Jr.
J. W. Winchester
Eduardo E. Wolf
E. J. Wu
P. Wynblatt
Roman Zaharchuk
Mary V. Zeller

AIChE Symposium Series

Number 201 1980 Volume 76

Published by

American Institute of Chemical Engineers

345 East 47th Street New York, New York 10017